

Supporting Information For:

Identification and Distribution of Vanadinite ($\text{Pb}_5(\text{V}^{5+}\text{O}_4)_3\text{Cl}$) in Lead Pipe Corrosion By-products

Tammie L. Gerke¹, Kirk G. Scheckel², and Michael R. Schock^{2*}

Twenty-two pages containing four appendices, three figures, and five tables:

Figure SI1. Diagram of the predominant aqueous vanadium species assuming dissolved vanadium species activities of 0.1 mg/L at 25°C, and an ionic strength of zero.

Appendix A. Analytical Methodology.

Appendix B. X-ray Diffraction – Powder and Micro

Table SI1. Most abundant crystalline lead phases identified by powder X-ray diffraction.

Table SI2. Linear combination fitting results for XANES spectra in Figure 1. Data presented as weighted percents over a fit range of -10 to 70 eV.

Figure SI2. μ -XRF map of vanadium concentrations for the selected region (indicated by black lines) for sample A6. The numbered location in the μ -XRF maps indicates the location of the representative μ -XRD trace. The μ -XRD trace is in blue and the main XRD identification peaks for vanadinite are indicated by gray transparent lines between 25 and 31 2θ . Based on the alignment of the main XRD vanadinite peak and a μ -XRD peak indicates the possible identification of vanadinite but this finding can not be confirmed with the μ -XRD data.

Appendix C. SEM-EDXA Elemental Maps.

Figure SI3. Thin-section image for sample A6. Arrows indicate regions where grains of vanadinite were identified. One representative region was imaged with secondary electrons at two different scales (arrow points to vanadinite grains) and elemental maps for vanadium (V), lead (Pb), and chlorine (Cl) were obtained.

Appendix D: Example Calculations for derivation of approximate upper limit for log K_{sp} and ΔG_f° for vanadinite

Table SI3. Water quality for utility A used to derive log K_{sp} for vanadinite.

Table SI4. Computation of limits to ΔG_f° for vanadinite.

Table SI5. Example computation from Geochemist's Workbench for ion activity product of vanadinite assuming equilibrium, for case with $\text{Cl}^- = 16 \text{ mg/L}$, $\text{V} = 0.002$ as VO_4^{3-} and $\text{Pb} = 0.010 \text{ mg/L}$ (Table SI3).

* Corresponding author phone: 513-569-7412; fax 513-569-7172 email: Schock.Michael@epa.gov

¹ Department of Geology, University of Cincinnati, Cincinnati, OH 45221-0013

² USEPA, NRMRL, 26 West Martin Luther King Drive, Cincinnati, OH 45268

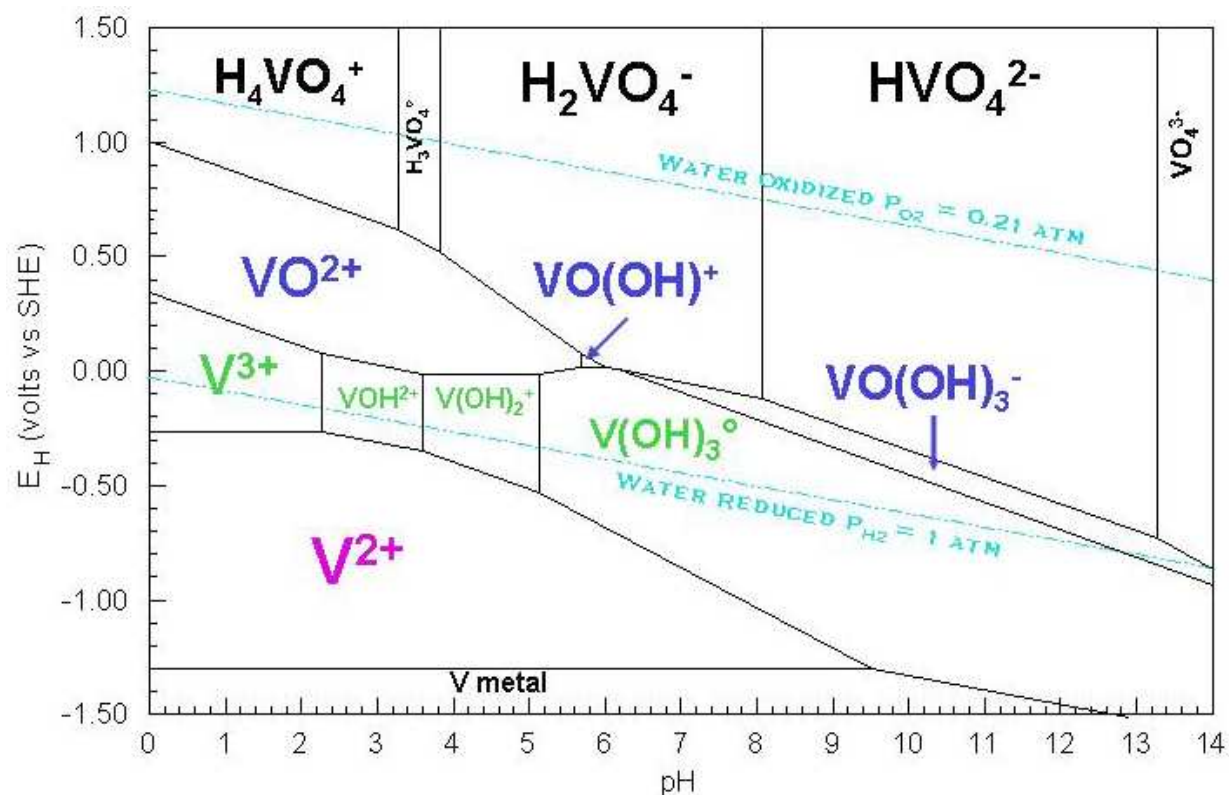


Figure SII. Diagram of the predominant aqueous vanadium species assuming dissolved vanadium species activities of 0.1 mg/L at 25°C, and an ionic strength of zero.

Appendix A. Analytical Methodology

Traditional Powder XRD

All samples were analyzed using a Scintag XDS-2000 theta-theta diffractometer system equipped with a Peltier detector using a Cu K α radiation at 40 kV and either 30 or 40 mA. The typical analysis used a 2θ range from 5° to 90°, with a 0.02° step, and a 2 second count time at each step. Alternative conditions were used occasionally to clarify certain spectral features. Crystalline phase identifications were made using Jade XRD software (Version 8.0, MDI Incorporated, Livermore, CA) and the International Center for Diffraction Data 2002 PDF-2 release, in general accordance with ASTM Standard Practices (1,2). Depending on the amount of sample available, the ground powders were either filled into a well in zero-background quartz

plates, or were evaporated in a slurry with AR-grade amyl acetate onto a flat zero-background quartz plate (Gem Dugout, State College, PA).

ICP-OES

Aliquots of samples were analyzed at the United States Geological Survey (USGS) facilities in Denver, Colorado in accordance with USGS procedures (3) using a Perkin Elmer/Sciex Elan 3000 spectrophotometer. The samples were analyzed for a wide spectrum of elements but only vanadium and lead concentrations are reported here (Table 1).

SEM

Secondary electron images and elemental maps were obtained using a JEOL 5800 Scanning Electron Microscope with an attached Link Analytical energy dispersive X-ray analyzer. The accelerating voltage was 20 keV and an average count time of three to five minutes was used to obtain all EDXA elemental maps. The magnification used ranged from approximately 100x to 500x and samples were carbon coated.

Synchrotron

Sample Preparations

Nineteen randomly selected lead corrosion by-product layers from 12 lead pipes representing seven of the eight distribution systems were processed for bulk XANES analysis (Table 1). A thin layer of prepared corrosion by-product material was smeared onto Kapton tape and folded back on itself.

All *in-situ* micro-X-ray fluorescence elemental maps (μ -XRF maps) corresponding micro-X-ray diffraction (μ -XRD) analyses, and XANES analyses were conducted using thin sections of three lead pipes with their corrosion by-products *in-situ* from two distribution systems (Table 1). These pipe samples were not the same as any of the samples utilized for the bulk XANES analysis. Thin sections were prepared by encasing segments of lead pipe in Buehler Epo Thin[®] Low Viscosity Epoxy, mounting them on quartz slides and polished to a thickness of approximately 35 microns. Each section was digitally photographed using a Canon G3 digital camera mounted to a copy stand.

Linear combination fitting refers to the process of selecting a multiple component fitting function (a Levenberg-Marquardt least-squares algorithm in this study) that minimizes the sum of the squares of residuals. During the fitting procedure, residual error (the normalized root square difference between the sample spectra and fitted data) was minimized by removal of non-essential reference components and continued until no net improvement of residual error was observed. The parameters of the theoretical function model are the desired physical descriptors of the measurements in which one attempts to fit the data to the model and report the parameter values (often as a weight or fractional percent of the total). The accuracy of the fitting procedure depends upon data quality and measured limits in addition to how well the reference standards actually represent the soil samples. We utilized a fit range of -10 to 70 eV for the XANES spectra which encompassed 289 data points and four variables. The best fitting scenarios, determined by the smallest residual error and the sum of all fractions being close to 1, are shown in Table SI2. A minimum of 2 components were necessary to fully describe any particular sample within 1% reproducible error indicating that two V species could be tested statistically

stringent. The fundamental source of fitting error is typically due to the limited number of actuators that afford a limited number of degrees of freedom for which, in our case, we restricted error significantly. The reference samples included in the principal component analysis and LCF fitting procedure included vanadinite, lenoblite, V(V) oxide, mixed V(IV,V) oxide, and V metal.

20-BM

Bulk XANES

V (5465 eV) K-XANES data were collected with electron storage ring operated at 7 GeV with a current of 101 mA. Three to five scans were collected at ambient temperature in fluorescence mode with a solid-state 13-element detector. A 0.5 mm pre-monochromator slit width and a Si(III) double crystal monochromator detuned by 10% to reject higher-order harmonics was employed. The beam energy was calibrated by assigning the first inflection of the absorption edge of vanadium metal foil to 5465 eV. Reference samples of various vanadium-rich phases were collected for comparison with the XANES spectra (Figure 1b; Table 2). The collected scans for a particular sample were averaged, the data were then normalized, and the background was removed by spline fitting using IFEFFIT (4).

20-ID

micro-XRF

X-ray micro-beam studies (fluorescence and diffraction) were performed at XOR/PNC 20-ID of the Advanced Photon Source (APS), Argonne National Laboratory (Argonne, IL) under standard operating conditions (7 GeV and ring current of 101 mA in top-up mode). μ -XRF maps were recorded using a multi-element solid-state Ge energy dispersive detector (Canberra). The

monochromatic beam energy was set at 13.1 KeV using a Si (111) channel-cut monochromator and the beam was focused to approximately 15 x 15 μm using rhodium-coated Kirkpatrick-Baez focusing optics. $\mu\text{-XRF}$ maps were obtained using various step sizes and counts per pixel. Micro regions of interest within the lead scales were selected for additional analyses ($\mu\text{-XRD}$ and XANES) based on the elemental data obtained from $\mu\text{-XRF}$ maps.

micro-XRD

A MAR 165 charge-coupled detector (CCD) was used for microcrystallography ($\mu\text{-XRD}$) studies and was positioned at approximately 190 mm from the sample. Two dimensional $\mu\text{-XRD}$ patterns were collected for 60 to 120 s at 15 KeV with a wavelength (λ) of 0.8265 Å. Two-dimensional diffractograms (2D Debye-Scherrer rings) were converted to one-dimensional 2θ scans using the software package Fit2D⁵

micro-XANES

V (5465 eV) K-XANES data were collected with electron storage ring operated at 7 GeV with a current of 101 mA. Three scans were collected at ambient temperature in fluorescence mode with a solid-state 13-element detector. A 0.5 mm pre-monochromator slit width and a Si(III) double crystal monochromator detuned by 10% to reject higher-order harmonics was employed. The beam energy was calibrated by assigning the first inflection of the absorption edge of vanadium metal foil to 5465 eV. Reference samples of various vanadium-rich phases were collected for comparison with the XANES spectra (Figure 1b; Table 2). The collected scans for a particular sample were averaged, the data were then normalized, and the background was removed by spline fitting using IFEFFIT (4).

Table SI1. Most abundant crystalline lead phases identified by powder X-ray diffraction.

Sample ID	Layer	Cerussite	Hydrocerussite	Plattnerite	Litharge	Pb ^{II} orthophosphate(s) Pb ₅ (PO ₄) ₃ (OH,Cl,F), Pb ₉ (PO ₄) ₆
		PbCO ₃	Pb ₃ (CO ₃) ₂ (OH) ₂	PbO ₂	PbO	
A1	L1			X		
	L2			X		
A2	L1			X		
	L2			X		
A3	L1			X		X
	L2			X		
	L3			X	X	
A4	L1			X		
	L2			X		
	L3			X		
	L4			X		
A5	L1			X		X
	L2		X			
	L3			X		
A6	L1					X
	L2			X		
	L3			X		
A7	L1			X		X
	L2					X
	L3				X	
B1	whole		X			
C1	L1					
	L2		X			
	L3		X			
D1	L1		X			
E1	L1	X				
	L2	X				
	L3	X				
F1	L1	X	X			
G1	L1			X		
H1	L1		X			
I1	L1	X				
	L2	X				
	L3	X				

Table S12. Linear combination fitting results for XANES spectra in Figure 1. Data presented as weighted percents over a fit range of -10 to 70 eV.

Sample	References				R-factor ^a
	Vanadinite	Lenoblite	V(V) Oxide	V(IV,V) Oxide	
A5 L1	91.4		8.6		0.002
D1 L1	89.8		10.2		0.005
G1 L1	92.6		7.4		0.004
A6 PtB	95.2		4.8		0.002
I1 PtH	98.1		1.9		0.002

^a R-factor = $[(\text{data-fit})^2]/[\text{data}^2]$

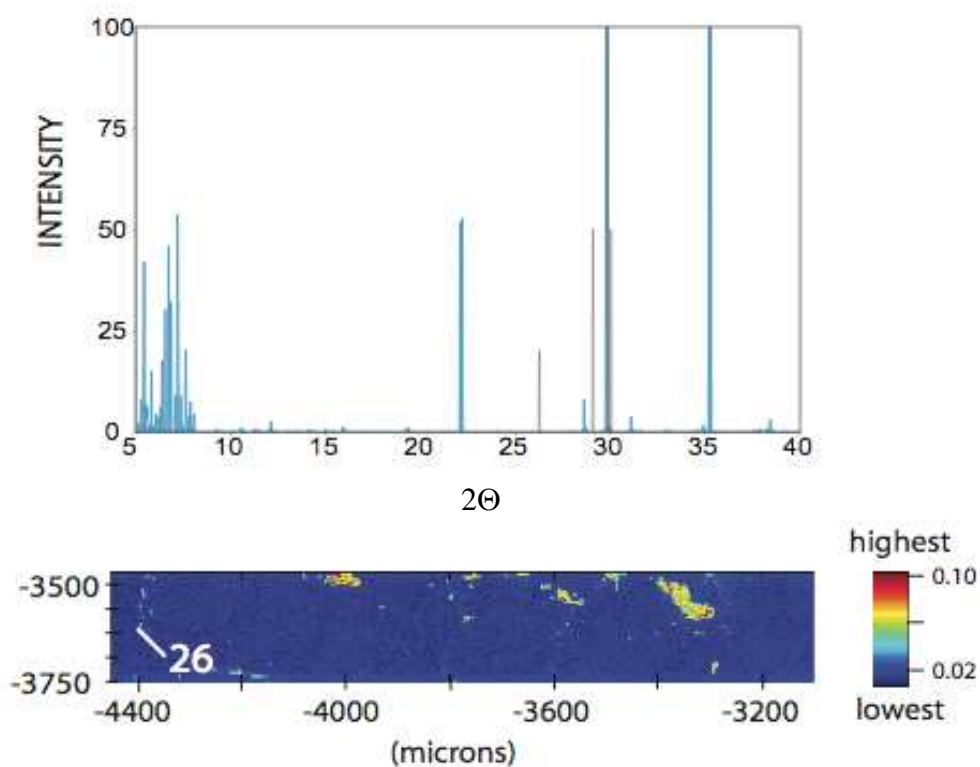


Figure SI2: Example μ -XRF map of vanadium concentrations for a selected region of sample A6. The numbered location in the μ -XRF maps indicates the location of the representative μ -XRD trace. The μ -XRD trace is in blue and the main XRD identification peaks for vanadinite are indicated by gray transparent lines between 25 and 31 2θ . This example shows typically poor agreement between the reference XRD vanadinite peaks and the μ -XRD pattern.

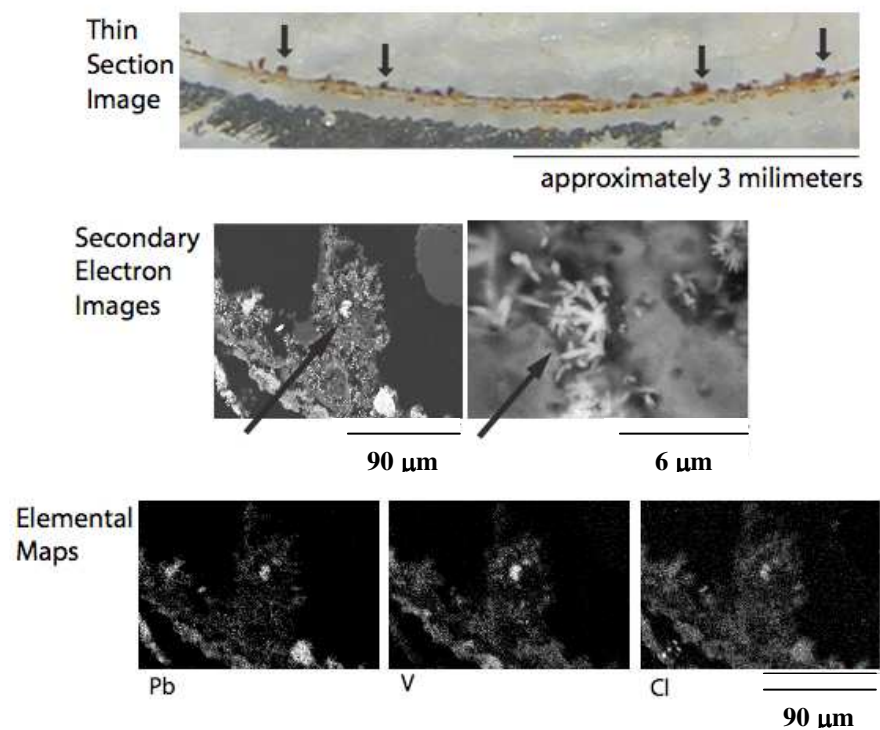


Figure SI3: Thin-section image for sample A6. Arrows indicate regions where grains of vanadinite were identified. One representative region was imaged with secondary electrons at two different scales (arrow points to vanadinite grains) and elemental maps for vanadium (V), lead (Pb), and chlorine (Cl) were obtained. Scales are provided for all images.

Appendix B: Example Calculations for derivation of approximate upper limit for log K_{sp} and ΔG_f° for vanadinite

Using the general background water chemistry and assumptions about the limits of the highly varying water matrix constituents (which would affect ionic strength and particularly lead speciation), a range of log K_{sp} and ΔG_f° values for presumed equilibrium with vanadinite can be calculated. The text discusses some important factors pertaining to the estimation of the dissolved lead(II) concentration in the water, and what assumptions were made here. In addition, there is a possibility that the dissolved lead(II) concentration was considerably over 200 micrograms per liter for prolonged periods of time at utility A, when reductive dissolution of the PbO_2 deposits were taking place. Two different logical paths can be taken with respect to this phenomenon, and they would result in different presumptions of total soluble lead for the modeling. On the one hand, there was a very high lead concentration during stagnation for several years, which could suggest that log K_{sp} for vanadinite would be much higher than is computed here. However, following the trend of analysis of V in the pipe deposits from this water system, indicates that the V concentrations in the scale appear to actually be increasing slightly with continued exposure to the phosphate treatment chemical, and when soluble lead release was lower, but background water redox conditions were stabilizing to lead(II)-orthophosphate precipitation and formation within the outer scale layers. Analyses of V-rich scales from other water systems for which reasonable estimates of redox and lead release conditions can be made with some confidence, further suggest that Pb concentrations need not be in the hundreds of micrograms per liter to form vanadinite. Thus, we have concluded that during the initial highly-plumbosolvent conditions of rampant reductive dissolution at this water

system, the scale removal rate physically constrained the ability of vanadinite to form and remain stable within the scale itself. Only further detailed lead speciation research in the laboratory and with future field investigations will really resolve this apparent paradox.

The computer program Geochemist's Workbench (Release 7, Rockware Inc., Golden, CO) was used to perform the speciation calculations (6). The temperature was assumed to be 25°C, because there are few reliable temperature functions for adjusting the lead and vanadium equilibrium constants to other temperatures. Sodium was used to balance charge, as it would have minimal impact on the actual fraction of the metals complexed. Equilibrium constants for vanadium species were used as furnished in the "thermo.dat" data file, and generally followed Wany and Goldhaber (1992) (7). Equilibrium constants for lead species were taken from NIST (2001) for aqueous complexes or from Schock et al. (1996) (8,9). The NIST formation constants for lead carbonate complexes are considerably smaller than those used for previous solubility computations by Schock et al. (9) and many references cited therein, which could be a source of bias in the estimation performed here. As noted, these computed values likely represent an approximate upper bound to the solubility of vanadinite, as during normal water usage and flow patterns in the premises, as well as with typical treatment and seasonal water variability, lead and vanadium concentrations are probably usually lower than the assumptions here. There is also some variability in the inorganic carbon concentration and pH over the year, so that adds more complication to handling all possible combinations of background constituent concentrations.

Table SI3. Water quality for utility A used to derive log K_{sp} for vanadinite.

Parameter	City A
pH	7.6
Total Alkalinity (mg/L as HCO_3)	74
E_h (est,volts vs SHE)	.700
<i>mg/L (in units indicated)</i>	
Aluminum	.08
Calcium	46
Chloride	16-89
Fluoride	1
Lead ($\mu\text{g/L}$)	7, 10, 15
Magnesium	9.9
Nitrate	13.3
Orthophosphate	2.3
Potassium	3
Silica	--
Sodium	16
Sulfate	54
Vanadium	.0009

Table SI4. Computation of limits to ΔG°_f for vanadinite.

$$K_{sp} = \{Pb^{2+}\}^5 \{VO_4^{3-}\}^3 \{Cl^-\} \quad \log K_{sp} = -[\Delta G^\circ_r / 5.7077]$$

$$R = 8.314E^{-3} \text{ kJ/mol} \times \text{deg}$$

kJ/mol

$\Delta G^\circ_f Cl^-$ **-131.23** Wanty & Goldhaber 1992

$\Delta G^\circ_f Pb^{2+}$ **-24.69**

$\Delta G^\circ_f VO_4^{3-}$ **-899.00** Wanty & Goldhaber 1992

Input Total Concentrations			Computed Activities			Computed log K _{sp}	Computed ΔG° _r	Computed ΔG° _f vanadinite
Cl ⁻	Pb ²⁺	V as VO ₄ ³⁻	Cl ⁻	Pb ²⁺	VO ₄ ³⁻			
City A Data								
89	0.007	0.002	-2.6456	-8.5072	-13.7804	-86.5228	493.8462	-3445.5
16	0.007	0.002	-3.3865	-8.5020	-13.7729	-87.2152	497.7982	-3449.5
89	0.010	0.002	-2.6468	-8.3493	-13.7804	-85.7345	489.3468	-3441.0
16	0.010	0.002	-3.3865	-8.3471	-13.7729	-86.4407	493.3776	-3445.1
89	0.015	0.002	-2.6468	-8.1732	-13.7804	-84.8540	484.3212	-3436.0
16	0.015	0.002	-3.3865	-8.1710	-13.7729	-85.5602	488.3520	-3440.0
Average:						-86.0546	491.1737	-3442.9

Table SI5. Example computation from Geochemist's Workbench for ion activity product of vanadinite assuming equilibrium, for case with $\text{Cl}^- = 16 \text{ mg/L}$, $\text{V} = 0.002$ as VO_4^{3-} and $\text{Pb} = 0.010 \text{ mg/L}$ (Table SI4).

Temperature =	25.0 C	Pressure =	1.013 bars
pH =	7.600	log fO2 =	-5.370
Eh =	0.7000 volts	pe =	11.8333
Ionic strength	=	0.005065	
Activity of water	=	0.999984	
Solvent mass	=	1.000000 kg	
Solution mass	=	1.000242 kg	
Solution density	=	1.013 g/cm3	
Chlorinity	=	0.000446 molal	
Dissolved solids	=	242 mg/kg sol'n	
Rock mass	=	0.000000 kg	
Carbonate alkalinity=		74.00 mg/kg as CaCO3	

No minerals in system.

Aqueous species	molality	mg/kg sol'n	act. coef.	log act.
HCO3-	0.001447	88.26	0.9277	-2.8722
Ca++	0.001037	41.54	0.7466	-3.1113
SO4--	0.0004802	46.12	0.7373	-3.4509
Cl-	0.0004438	15.73	0.9254	-3.3865
Mg++	0.0003770	9.160	0.7552	-3.5456
Na+	0.0002186	5.025	0.9270	-3.6932
NO3-	0.0002105	13.05	0.9254	-3.7103
CO2 (aq)	7.832e-005	3.446	1.0000	-4.1062
K+	7.558e-005	2.954	0.9254	-4.1553
CaSO4	5.724e-005	7.790	1.0000	-4.2423
F-	5.058e-005	0.9607	0.9262	-4.3293
CaHCO3+	1.865e-005	1.885	0.9287	-4.7615
MgSO4	1.702e-005	2.048	1.0000	-4.7690
HPO4--	1.287e-005	1.235	0.7373	-5.0227
MgHCO3+	4.219e-006	0.3599	0.9270	-5.4077
H2PO4-	4.126e-006	0.4000	0.9270	-5.4174
CaHPO4	4.035e-006	0.5489	1.0000	-5.3942
CO3--	3.273e-006	0.1963	0.7397	-5.6161
CaCO3	3.080e-006	0.3082	1.0000	-5.5115
Al (OH) 4-	2.825e-006	0.2683	0.9270	-5.5819
MgHPO4	2.195e-006	0.2640	1.0000	-5.6585
Sr++	2.100e-006	0.1839	0.7420	-5.8074
CaCl+	1.719e-006	0.1298	0.9270	-5.7978
CaNO3+	1.297e-006	0.1324	0.9270	-5.9200
MgF+	9.067e-007	0.03925	0.9270	-6.0755
MgCO3	5.696e-007	0.04802	1.0000	-6.2444
CaF+	4.926e-007	0.02910	0.9270	-6.3404
CaPO4-	4.456e-007	0.06017	0.9270	-6.3840
OH-	4.431e-007	0.007534	0.9262	-6.3868
NaSO4-	3.825e-007	0.04552	0.9270	-6.4503
NaHCO3	3.661e-007	0.03075	1.0000	-6.4364
KSO4-	1.902e-007	0.02570	0.9270	-6.7537
MgCl+	1.783e-007	0.01065	0.9270	-6.7818
MgPO4-	1.639e-007	0.01954	0.9270	-6.8184

SrSO4	1.099e-007	0.02018	1.0000	-6.9589
Al (OH) 3	6.428e-008	0.005013	1.0000	-7.1919
MgH2PO4+	3.711e-008	0.004500	0.9270	-7.4635
SrHCO3+	3.404e-008	0.005058	0.9270	-7.5010
PbCO3 (aq)	3.387e-008	0.009047	1.0000	-7.4702
NaHPO4-	2.931e-008	0.003486	0.9270	-7.5659
H+	2.690e-008	2.710e-005	0.9338	-7.6000
MgOH+	1.979e-008	0.0008175	0.9270	-7.7364
VO2 (OH) 2-	1.504e-008	0.001759	0.9270	-7.8556
KHPO4-	7.853e-009	0.001060	0.9270	-8.1379
CaOH+	6.806e-009	0.0003885	0.9270	-8.2000
Pb++	6.080e-009	0.001259	0.7397	-8.3471
SrHPO4	5.492e-009	0.001008	1.0000	-8.2603
O2 (aq)	5.378e-009	0.0001721	1.0013	-8.2688
PbOH+	4.851e-009	0.001087	0.9270	-8.3471
SrCO3	2.420e-009	0.0003572	1.0000	-8.6162
VO3OH--	2.139e-009	0.0002479	0.7373	-8.8022
NaCl	2.094e-009	0.0001223	1.0000	-8.6791
SrNO3+	2.065e-009	0.0003089	0.9270	-8.7181
Al (OH) 2+	2.015e-009	0.0001229	0.9270	-8.7287
HF	1.738e-009	3.476e-005	1.0000	-8.7599
NaCO3-	1.690e-009	0.0001403	0.9270	-8.8050
PbHCO3+	1.530e-009	0.0004103	0.9270	-8.8482
NaF	1.253e-009	5.258e-005	1.0000	-8.9022
HSO4-	9.441e-010	9.162e-005	0.9270	-9.0579
PbSO4 (aq)	7.799e-010	0.0002364	1.0000	-9.1080
Mg2CO3++	7.620e-010	8.275e-005	0.7420	-9.2476
KCl	7.424e-010	5.534e-005	1.0000	-9.1293
SrF+	4.426e-010	4.717e-005	0.9270	-9.3870
PO4---	3.684e-010	3.498e-005	0.5034	-9.7317
Pb (CO3) 2--	3.319e-010	0.0001086	0.7373	-9.6114
N2 (aq)	2.051e-010	5.745e-006	1.0000	-9.6880
AlF2+	1.405e-010	9.128e-006	0.9270	-9.8852
SrPO4-	9.848e-011	1.798e-005	0.9270	-10.0396
PbCl+	7.932e-011	1.924e-005	0.9270	-10.1336
AlF3	7.660e-011	6.431e-006	1.0000	-10.1158
Pb (OH) 2 (aq)	5.793e-011	1.397e-005	1.0000	-10.2371
PbHPO4	5.370e-011	1.628e-005	1.0000	-10.2700
NaOH	5.220e-011	2.087e-006	1.0000	-10.2823
SrH2PO4+	3.613e-011	6.668e-006	0.9270	-10.4751
PbF+	2.794e-011	6.319e-006	0.9270	-10.5867
H3PO4	1.349e-011	1.322e-006	1.0000	-10.8698
AlHPO4+	9.638e-012	1.185e-006	0.9270	-11.0489
AlF++	9.427e-012	4.333e-007	0.7420	-11.1552
AlOH++	9.330e-012	4.103e-007	0.7420	-11.1597
KOH	9.110e-012	5.110e-007	1.0000	-11.0405
SrOH+	3.539e-012	3.702e-007	0.9270	-11.4840
VO (OH) 3	3.519e-012	4.151e-007	1.0000	-11.4535
Pb (SO4) 2--	2.257e-012	9.009e-007	0.7373	-11.7789
PbPO4-	2.255e-012	6.812e-007	0.9270	-11.6798
AlF4-	9.720e-013	1.001e-007	0.9270	-12.0453
PbH2PO4+	5.861e-013	1.783e-007	0.9270	-12.2649
HF2-	2.777e-013	1.083e-008	0.9270	-12.5894
Mg2OH+++	2.619e-013	1.718e-008	0.5314	-12.8565
PbCl2 (aq)	4.571e-014	1.271e-008	1.0000	-13.3400
VO4---	3.351e-014	3.850e-009	0.5034	-13.7729
PbF2	2.977e-014	7.298e-009	1.0000	-13.5262

Al+++	2.780e-014	7.500e-010	0.5379	-13.8252
Pb(OH) 3-	2.488e-014	6.423e-009	0.9270	-13.6371
AlSO4+	5.840e-015	7.184e-010	0.9270	-14.2665
AlF5--	4.242e-015	5.173e-010	0.7373	-14.5048
NO2-	1.395e-015	6.415e-011	0.9254	-14.8891
Pb2OH+++	6.789e-016	2.928e-010	0.4721	-15.4942
VO2HPO4-	6.719e-016	1.202e-010	0.9270	-15.2057
VO2+	1.902e-016	1.578e-011	0.9270	-15.7536
Al (SO4) 2-	1.617e-016	3.543e-011	0.9270	-15.8241
AlH2PO4++	1.537e-016	1.905e-011	0.7420	-15.9428
VO2F	2.711e-017	2.763e-012	1.0000	-16.5668
PbCl3-	1.609e-017	5.042e-012	0.9270	-16.8265
HCl	8.195e-018	2.987e-013	1.0000	-17.0865
H2F2	8.096e-018	3.238e-013	1.0000	-17.0918
VO2 (HPO4) 2---	5.109e-018	1.404e-012	0.5034	-17.5897
Pb(OH) 4--	3.057e-018	8.411e-013	0.7373	-17.6471
VO2SO4-	1.661e-018	2.972e-013	0.9270	-17.8126
VO2F2-	2.595e-019	3.138e-014	0.9270	-18.6188
AlF6---	1.564e-019	2.204e-014	0.5034	-19.1038
Pb3 (OH) 4++	5.936e-020	4.092e-014	0.7166	-19.3713
HNO2	5.390e-020	2.533e-015	1.0000	-19.2684
VO2H2PO4	2.763e-020	4.971e-015	1.0000	-19.5586
H2SO4	2.172e-020	2.130e-015	1.0000	-19.6631
Al2 (OH) 2++++	2.170e-020	1.908e-015	0.3459	-20.1247
PbCl4--	4.163e-021	1.452e-015	0.7373	-20.5130
VO2F3--	3.173e-022	4.439e-017	0.7373	-21.6309
Mg4 (OH) 4++++	1.068e-023	1.764e-018	0.3459	-23.4326
VOOH+	1.253e-024	1.052e-019	0.9270	-23.9348
Pb4 (OH) 4++++	1.121e-024	1.005e-018	0.2632	-24.5298
Al3 (OH) 4 (5+)	6.075e-025	9.048e-020	0.1903	-24.9370
H4P2O7	4.493e-026	7.994e-021	1.0000	-25.3475
VO++	1.842e-026	1.232e-021	0.7420	-25.8644
VOF+	4.451e-027	3.825e-022	0.9270	-26.3844
VOSO4	1.450e-027	2.364e-022	1.0000	-26.8385
VOF2	6.837e-029	7.172e-024	1.0000	-28.1652
(VO) 2 (OH) 5-	3.843e-031	8.411e-026	0.9270	-30.4483
VOF3-	1.252e-031	1.551e-026	0.9270	-30.9354
Pb6 (OH) 8++++	4.478e-033	6.175e-027	0.3065	-32.8625
Al13O4 (OH) 24 (7+)	1.505e-034	1.238e-028	0.0387	-35.2348
VOF4--	2.391e-035	3.417e-030	0.7373	-34.7538
ClO4-	2.503e-036	2.489e-031	0.9262	-35.6348
V (OH) 2+	4.619e-039	3.923e-034	0.9270	-38.3684
Pb++++	4.487e-042	9.294e-037	0.3065	-41.8617
VOH++	2.441e-042	1.658e-037	0.7420	-41.7420
H2 (aq)	1.049e-042	2.115e-039	1.0013	-41.9785
(VO) 2 (OH) 2++	8.495e-044	1.426e-038	0.7420	-43.2004
V+++	1.518e-047	7.733e-043	0.5034	-47.1167
VSO4+	1.452e-048	2.134e-043	0.9270	-47.8710
NH4+	5.354e-056	9.656e-052	0.9246	-55.3053
NH3	1.041e-057	1.772e-053	1.0000	-56.9827
NH4SO4-	1.646e-058	1.877e-053	0.9270	-57.8166
V2 (OH) 2++++	4.259e-083	5.787e-078	0.3459	-82.8317
HS-	1.499e-133	4.954e-129	0.9262	-132.8576
H2S (aq)	3.107e-134	1.059e-129	1.0000	-133.5076
CH4 (aq)	9.054e-139	1.452e-134	1.0013	-138.0426
S--	9.306e-140	2.983e-135	0.7420	-139.1608
CH3COO-	3.000e-144	1.771e-139	0.9277	-143.5554

MgCH3COO+	1.593e-146	1.327e-141	0.9270	-145.8308
HCH3COO	3.989e-147	2.395e-142	1.0000	-146.3991
NaCH3COO	3.705e-148	3.039e-143	1.0000	-147.4312
CaCH3COO+	1.530e-148	1.516e-143	0.9270	-147.8483
SrCH3COO+	6.433e-149	9.432e-144	0.9270	-148.2245
AlCH3COO++	4.079e-155	3.508e-150	0.7420	-154.5190
S2--	2.970e-238	1.904e-233	0.7373	-237.6595
S4--	0.0000	0.0000	0.7373	-300.0000
S3--	0.0000	0.0000	0.7373	-300.0000
Ca(O-phth)	0.0000	0.0000	1.0000	-300.0000
Al(O-phth)+	0.0000	0.0000	0.9270	-300.0000
H2(O-phth)	0.0000	0.0000	1.0000	-300.0000
Na(O-phth)-	0.0000	0.0000	0.9270	-300.0000
H(O-phth)-	0.0000	0.0000	0.9270	-300.0000
S6--	0.0000	0.0000	0.7373	-300.0000
S5--	0.0000	0.0000	0.7373	-300.0000
Al(O-phth)2-	0.0000	0.0000	0.9270	-300.0000
(O-phth)--	0.0000	0.0000	0.7373	-300.0000

Mineral saturation states

	log Q/K		log Q/K
<hr/>			
Fluorapatite	21.2905s/sat	Arcanite	-10.0726
Hydroxyapatite	11.2984s/sat	MHSH(Mg1.5)	-10.3354
Chloropyromorphi	6.0019s/sat	Portlandite	-10.4887
Pyromorphite-Cl	5.9999s/sat	Ca(OH)2(c)	-10.4887
Whitlockite	5.7210s/sat	Thenardite	-10.6014
Vanadinite	2.5594s/sat	MgSO4(c)	-12.0182
Plumbogummite	1.4644s/sat	Gaylussite	-12.2707
Gibbsite	1.0145s/sat	Pirssonite	-12.4334
Dolomite	0.2780s/sat	Sr(NO3)2^4H2O	-13.2457
Dolomite-ord	0.2780s/sat	SrCl2^6H2O	-13.2519
Diaspore	0.2231s/sat	KNaCO3^6H2O	-13.4433
Strontianite	0.0037s/sat	Sr(NO3)2(c)	-13.5726
Calcite	-0.0965	Mg2Cl(OH)3^4H2O	-13.7867
Pyromorphite-OH	-0.1383	Mercallite	-13.8311
Pb3(PO4)2(c)	-0.2207	Antarcticite	-13.9971
Aragonite	-0.2614	Kainite	-14.4305
Cerussite	-0.4336	Plumbonacrite	-14.5738
Pb9(PO4)6	-0.6202	Plumbonacrite	-14.5738
Boehmite	-0.6213	CaCl2^4H2O	-14.7763
Hydroxypyromorph	-0.6516	Bischofite	-14.8477
Fluorite	-0.8111	V2O5(c)	-14.8530
Pb4O(PO4)2(c)	-0.8560	Hinsdalite	-14.9410
Pb3(PO4)2	-1.0467	SrCl2^2H2O	-15.1033
Monohydrocalcite	-1.0904	Hydromagnesite	-15.1771
Magnesite	-1.2543	MgOHCl	-15.3795
Dolomite-dis	-1.2664	Bloedite	-15.5706
CaHPO4^2H2O	-1.5768	MgV2O6(c)	-15.8471
PbHPO4(c)	-1.9411	SrCl2^H2O	-16.5796
Gypsum	-2.1189	K2CO3^3/2H2O	-17.0557
Hydrocerussite	-2.2333	Sr(OH)2(c)	-17.1649
Hydrocer (aged)	-2.2536	MgCl2^4H2O	-17.7760
Dawsonite	-2.2693	CaCl2^2H2O	-17.9805
Hydrocer (aged)	-2.2836	CaCl2^H2O	-18.1153
Anhydrite	-2.2970	Ca3V2O8(c)	-18.6834
Celestite	-2.8271	SrCl2(c)	-19.7417

Bassanite	-2.9259	Lime	-20.6053
Pb3(CO3)2(OH)2	-3.0436	Hydrophilite	-21.7030
CaSO4 ^{1/2} H2O(bet	-3.0945	Carnallite	-22.3184
Corundum	-3.4342	MgCl2 ² H2O	-23.2133
Plattnerite	-3.4956	Ca2Cl2(OH)2 ² H2O	-24.1339
SrHPO4(c)	-3.8302	Na3H(SO4)2	-24.7899
Plattnerite	-3.8416	MgCl2 ² H2O	-26.5659
Nesquehonite	-3.9530	V2O4(c)	-29.8989
Anglesite	-3.9842	SrO(c)	-31.7271
MgF2(c)	-4.0257	KMgCl3 ² H2O	-32.0032
Hydrocer(fresh)	-4.3036	Chloromagnesite	-32.3228
Berlinite	-4.3718	Burkeite	-33.9868
Brucite	-4.7845	KMgCl3	-39.3094
Epsomite	-5.1840	Al2(SO4)3 ⁶ H2O	-40.2659
Hexahydrite	-5.4207	Ca4Cl2(OH)6 ¹³ H2	-42.0248
Huntite	-5.5920	Tachyhydrite	-47.9659
Pentahydrite	-5.7615	Al2(SO4)3	-57.7270
SrF2(c)	-5.9276	V2O3(c)	-58.5712
Leonhardtite	-6.1500	PbF2(c)	-58.9134
Kieserite	-6.8867	K8H4(CO3)6 ³ H2O	-63.3675
Artinite	-7.0985	Graphite	-70.0192
Kalicinite	-7.3594	V3O5(c)	-72.7217
Alunite	-7.5942	V4O7(c)	-88.7502
Sylvite	-8.5012	Misenite	-92.4178
Halite	-8.6725	Sulfur-Rhmb	-99.4816
Spinel	-8.7887	Galena	-118.7591
Pb2Cl2CO3	-9.1213	(VO)3(PO4)2(c)	-121.2701
Ca2V2O7(c)	-9.3609	V	-125.0586
Mirabilite	-9.7461	SrS(c)	-148.3854
CaV2O6(c)	-9.7724	O-phth acid(c)	-554.7864

Gases	fugacity	log fug.

Steam	0.03131	-1.504
CO2(g)	0.002219	-2.654
O2(g)	4.268e-006	-5.370
N2(g)	3.139e-007	-6.503
H2(g)	1.360e-039	-38.867
H2S(g)	3.323e-133	-132.479
CH4(g)	5.993e-136	-135.222
S2(g)	1.381e-213	-212.860

Original basis	total moles	In fluid		Sorbed		Kd
		moles	mg/kg	moles	mg/kg	L/kg

Al+++	2.89e-006	2.89e-006	0.0780			
Ca++	0.00112	0.00112	45.0			
Cl-	0.000446	0.000446	15.8			
F-	5.20e-005	5.20e-005	0.987			
H+	6.29e-005	6.29e-005	0.0634			
H2O	55.5	55.5	1.00e+006			
HCO3-	0.00156	0.00156	94.9			
HPO4--	2.39e-005	2.39e-005	2.29			
K+	7.58e-005	7.58e-005	2.96			
Mg++	0.000402	0.000402	9.77			
NO3-	0.000212	0.000212	13.1			

Na+	0.000219	0.000219	5.04
O2(aq)	1.35e-008	1.35e-008	0.000431
Pb++	4.77e-008	4.77e-008	0.00987
SO4--	0.000555	0.000555	53.3
Sr++	2.25e-006	2.25e-006	0.197
V+++	1.72e-008	1.72e-008	0.000875

Elemental composition	In fluid		Sorbed		
	total moles	moles	mg/kg	moles	mg/kg

Aluminum	2.892e-006	2.892e-006	0.07800		
Calcium	0.001124	0.001124	45.02		
Carbon	0.001555	0.001555	18.68		
Chlorine	0.0004457	0.0004457	15.80		
Fluorine	5.198e-005	5.198e-005	0.9873		
Hydrogen	111.0	111.0	1.119e+005		
Lead	4.766e-008	4.766e-008	0.009873		
Magnesium	0.0004023	0.0004023	9.775		
Nitrogen	0.0002118	0.0002118	2.966		
Oxygen	55.52	55.52	8.880e+005		
Phosphorus	2.392e-005	2.392e-005	0.7406		
Potassium	7.578e-005	7.578e-005	2.962		
Sodium	0.0002194	0.0002194	5.043		
Strontium	2.254e-006	2.254e-006	0.1975		
Sulfur	0.0005552	0.0005552	17.79		
Vanadium	1.718e-008	1.718e-008	0.0008752		

References

- (1) ASTM. **2003**. Standard Practices for Sampling Water-Formed Deposits. Volume 11.02, D 887-82. American Society for Testing and Materials, Conshohocken, PA.
- (2) ASTM. **2003**. Standard Practices for Identification of Crystalline Compounds in Water-Formed Deposits by X-Ray Diffraction. Volume 11.02, D 934-80. American Society for Testing and Materials, Conshohocken, PA.
- (3) Lamothe, P. J.; Meier, A. L.; Wilson, S. A. The determination of forty elements in aqueous samples by inductively coupled plasma-mass spectrometry, Ch. H In *Analytical methods for chemical analysis of geologic and other materials*, U.S. Geological Survey, Open File Report 02-223; U.S. Geological Survey: Denver, CO, 2002.
- (4) Ravel, B.; Newville, M. ATHENA, ARTEMIS, HEPHAESTUS: data analysis for X-ray absorption spectroscopy using IFEFFIT. , *J. Synchrotron Rad.* **2005**, *12*, 537-541.
- (5) Hammersley, A., *ESRF* **2001**, *10* (132).
- (6) Bethke, C. M.; Yeakel, S. *The Geochemist's Workbench[®] Release 7.0 Reference Manual*; Rockware, Inc.: Golden, CO, 2007.
- (7) Wanty, R. B.; Goldhaber, M. B. Thermodynamics and kinetics of reactions involving vanadium in natural systems: Accumulation of vanadium in sedimentary rocks, *Geochim. Cosmochim. Acta* **1992**, *56* (4), 1471-1483.

- (8) National Institute of Standards and Technology *NIST Standard Reference Database 46: NIST Critically Selected Stability Constants of Metal Complexes Database, Version 6.0 for Windows*; U.S. Department of Commerce: Gaithersburg, MD, 2001.
- (9) Schock, M. R.; Wagner, I.; Oliphant, R. The Corrosion and Solubility of Lead in Drinking Water, In *Internal Corrosion of Water Distribution Systems*; Second ed.; AWWA Research Foundation/TZW: Denver, CO, 1996; pp 131-230.